Journal of Robotics and Control (JRC)
Volume 3, Issue 5, September 2022
ISSN: 2715-5072, DOI: 10.18196/jrc.v3i5.16316

Interaction Motion Control on Tri-finger Pneumatic Grasper using Variable Convergence Rate Prescribed Performance Impedance Control with Pressure-based Force Estimator

Addie Irawan [1]*, Mohd Iskandar Putra Azahar [2], Dwi Pebrianti [3]
[1, 2] Robotics, Intelligent Systems & Control Engineering (RISC) Research Group, Faculty of Electrical & Electronics Engineering Technology, Universiti Malaysia Pahang, 26600 Pekan, Pahang, Malaysia
[3] Department of Mechanical and Aerospace Engineering, Kulliyah of Engineering, International Islamic University Malaysia, 50728 Kuala Lumpur, Malaysia
Email: [1] addieirawan@ump.edu.my, [2] iskandarputra1995@gmail.com, [3] dwipebrianti@iium.edu.my
*Corresponding Author

Abstract— **Pneumatic robot is a fluid dynamic based robot system which possesses immense uncertainties and nonlinearities over its electrical driven counterpart. Requirement for dynamic motion handling further challenged the implemented control system on both aspects of interaction and compliance control. This study especially set to counter the unstable and inadaptable proportional motions of pneumatic robot grasper towards its environment through the employment of Variable Convergence Rate Prescribed Performance Impedance Control (VPPIC) with pressure-based force estimation (PFE). Impedance control was derived for a single finger of Tri-finger Pneumatic Grasper (TPG) robot, with improvement being subsequently made to the controller's output by appropriation of formulated finite-time prescribed performance control. Produced responses from exerted pressure of the maneuvered pneumatic piston were then recorded via derived PEE with adherence to both dynamics and geometry of the designated finger. Validation of the proposed method was proceeded on both circumstances of human hand as a blockage and ping-pong ball as methodical representation of a fragile object. Developed findings confirmed relatively uniform force sensing ability for both proposed PEE and load sensor as equipped to the robot's fingertip with respect to the experimented thrusting and holding of a human hand. Sensing capacity of the estimator has also advanced beyond the fingertip to enclose its finger in entirety. Whereas stable interaction control at negligible oscillation has been exhibited from VPPIC against the standard impedance control towards gentle and compression-free handling of fragile objects. Overall positional tracking of the finger, thus, justified VPPIC as a robust mechanism for smooth operation amid and succeed direct object interaction, notwithstanding its transcendence beyond boundaries of the prescribed performance constraint.**

Keywords— Pneumatic robot; Compliant and impedance control; Prescribed performance control; Force estimation.

I. INTRODUCTION

Also goes by the name *soft-paradigm*, environment adaption within robot operation has been highly essential towards interactions with fragile applications or materials. Industrial robots for surgical, medical and rehabilitation applications further required immensely skillful mastery control design to guarantee a robust and safe operation between humans and robots. As such, various industrial and scholastic efforts on compliant control design of a robot system were undertaken through dissimilar strategic implementations against the system's dynamics [1-6]. Disclosed aspiration towards a safe and stable robot-environment interaction further popularized the employment of impedance control by [7] in acquiring key components for the robot's control system. High-performance joint force/torque control as the basis, such elastic model control system has also uncovered potential extendibility through embedment of adaptive elements for the desired physical motions corresponding installed wrenches on the robot [8].

Recent problem astounding high-precision assembly of the manufacturing industry was primarily resolved through the implementation of commercial compliant systems as configured with high gearing and joint-level torque sensing such as the complex Cartesian machines and lightweight robots. However, such systems are limited to sizable application which are relatively complex and costly in deployment. On the other hand, fluid dynamics systems with the like of pneumatic actuator could effectively handle high force operations for an extensive interval at the uncertain of air compressibility, parametric uncertainties, and nonlinearities. Motion precision of a robot system further required targeted configuration under such arrangement considering the encountered difficulties for sustainable performance accuracy and stability [9, 10]. These constraints, thus, demoted the efficiency in motion control upon handling highly sensitive and dynamic operations like interactive motions. Additional issue as faced by heavy-duty industrial applications then unearthed insufficient sensitivity, anti-noise, and anti-vibration across specifications of a comprehensive sensory setup. Majority of the sensory arrangement across contemporary medium scale robots have utilized force sensors as mounted on specific regions such as the tips, joints and body for external force detection [11-14], alongside the complementation of alternative sensory approaches such as vision sensors [15-18]. Nevertheless, readied hydraulic and pneumatic robots for such heavy-duty industrial tasks would require additional setup and monetary

investment for the installation of built-in force sensors. Complex mechanical structure of default robotic design then concurred the impractical, inefficient and difficult nature of installing build-to-order contact sensing devices [19]. While marketed pneumatic heavy-duty systems were particularly designed to handle tough and rigid objects, their potential in grasping large-scale fragile objects such as boxes, thin fiber-based materials or pallets with soft surface structure should not be overlooked. The prospect was, thus, explored through employment of a compliant interaction control with component of impedance control for gentle and defect-free object handling.

Mechanical impedance control can be fundamentally divided into two categories; namely reference trajectory adjustment and variable impedance adaptation [3]. Adaptive impedance control was especially proposed by Wei *et al.* to reduce the structural damage as rendered by the harvesting robot to apples through implementation of reference model approaches as adjustment position value on the impedance controller output. The system's behaviors comprising both speed and deceleration in picking towards modelling of environmental stiffness, as well as the grasping force on an unchanged environmental stiffness and position were hereby studied. Situations of varying environmental stiffness and dynamically adjustable positions were also conditioned [20-23]. Notably, such changeable and uncertain circumstances were seemingly unadaptable by the traditional impedance control[7]. Prevailed inspiration on potential designing of adaptive variable impedance control upon excellent parametric optimization, thus, propelled far-reaching scholastic efforts since the method's inception through various modification, adoption and integration of adjacent control law, algorithms, and intelligent systems as per reported in [24-28]. An example is hereby observed on the work from Xu *et al.* which emphasized a robot's Cartesian input adjustment by adoption of an adaptive impedance control with self-tuning stiffness [3]. On the other hand, iterative learning approach was proposed by Ting and Aiguo for an improved impedance control on the upper-limb rehabilitation robot to achieve appropriate contacts during therapeutic operation [29]. The approach was then contrasted in the work of Izadbakhsh *et al.* on the introduction of Szász–Mirakyan operator as a tuning mechanism for internal impedance in guaranteeing enhanced interaction control [30]. In the case of Ji *et al.* where damping was endorsed as a designed parameter, an apple's biological characteristics ascertained using the Burgers model has been applied above conceptual paradigm of Hertz contact theory towards establishment of force model in fruit grasping [31]. Moreover, integration of impedance control and state observer on a three-fingered robotic hand was established by [32]. Emphasizing a diverging ground to the dynamic and self-tuning approach of impedance control, positional set-point centering independent finger was hereby adapted for joint impedance control following transformation in the kinematics model with respect to the measured response of each structural joint.

Other apparent shortcomings concerning impedance control of pneumatic robots as encountered within both pressure state and nonlinearity of the pneumatic actuator further steered considerable research towards duplication of comparable robustness and optimal impedance against abutting robotic counterparts. Case in point being the work of [33] on differentiated stiffness of its impedance control over the referenced pressure dynamics of a servo pneumatic and sliding mode control across an array of control input design. Echoing the work of [8] centering employment of torque-based impedance for torque control design; impedance model was adopted by Turkseven and Ueda as the desired model reference in pneumatic position control design [34]. Sensory sensitivity of force feedback throughout heavy-duty industrial applications such as the Tri-finger Pneumatic Grasper (TPG) robot unit is particularly prominent as impedance input corresponding experienced complications for adequate direct force sensor.

Subsequent emphasis is placed on the significance of tracking error towards impedance control performance. Following changes in dynamic reference input from the impedance controller, delayed timing and decreased precision in finger position would potentially occur from an increased transformational frequency of reference input. Likewise, an increased complexity of outer-loop controllers such as the position control system would then contribute a larger number of tuning parameters. Identified shortcoming was consequentially tackled through incorporation of prescribed performance control (PPC) as the error transformation technique to exhibited changes in error tracking via the impedance controller, alongside the employment of position controller input as an outer controller [8]. The approach was primarily introduced by Bechlioulis and Rovithakis for enhanced practicality with marginally diminished operational drawbacks [35]. On current note, finite-time method has been reflectively adopted from other scholastic predecessors to overcome the impractical selection of exponential convergence rate as per demonstrated within earlier works of [35-38]. On the attempt of extension method for transformed error restraining, barrier Lyapunov function (BLF) was modified and improved through embedment of novel techniques by [39] in guaranteeing systematic stability facing transformed error which surpassed the established boundary. Readjusting performance function based approach upon fine-tuning of prescribed performance function with accordance to the prescribed constraints on error tracking was additionally proposed by [40]. Comparable modification and association of PPC to data driven methods were also ventured for improved precision of model-based control systems [41, 42]. Alternatively, a diverged outlook was exempted by Luo *et al*., Cao *et al.* and Bu on the adaptation of intelligent control towards enhance sensory tracking of said error transformation control approach [43-45]. With a wide range of formulations being undertaken towards PPC, in-depth priority was further relocated to the system's PPF on its immense potential for enhanced real-time applications [46-54].

Presented discussion ultimately motivated the current exploration for improved impedance control on heavy-duty TPG through proposed implementation of Variable Convergence Rate Prescribed Performance Impedance Control (VPPIC) following integration of position-based impedance control as the feedforward sub-controller to the

Variable Convergence Rate Prescribed Performance Control. This study then contributed the development of pressure-based force estimation (PFE) as the force estimator which accounted the pressure of pneumatic actuator, kinematics, and dynamics of TPG's finger. Upon realizing challenge concerning the handling of fragile objects among heavy-duty industrial robots like TPG which were specifically designed for burdensome applications, undertaken experimentation was, therefore, aimed to enable stable and precise interactive motional control at the system's finger for increased reliability towards considerably delicate object grasping. As such, comparison was fundamentally made between the derived VPPIC method and the standard position-based impedance control via an identical platform for analysis and validation of the proposed approach.

Presented paper has been organized as follows: Section II discusses an overview of TPG system and its configuration. Discussion regarding the proposed interaction control strategy which encompassed derivation of the position-based impedance control with integration of PPE technique on a TPG's fingertip and formulation of the proposed VPPIC through employment of the proposed variable convergence rate prescribed performance function (VCR-PPF) has been further outlined in Section III. Section IV subsequently describes the developed analyses and results on both experimental setup and calibration of the proposed force estimator. Last but not least, the paper is compendiously concluded in Section V.

II. TRI-FINGER PNEUMATIC GRASPER SYSTEM

Tri-finger Pneumatic Gripper (TPG) was designed and customized as a tool for the FANUC Robot S-430iF as shown in Fig.1. The robot was donated by Perusahaan Otomobil Kedua Sendirian Berhad (Perodua) Malaysia to the teaching and learning laboratory of Faculty of Electrical and Electronics Engineering Technology (FTKEE), Universiti Malaysia Pahang.

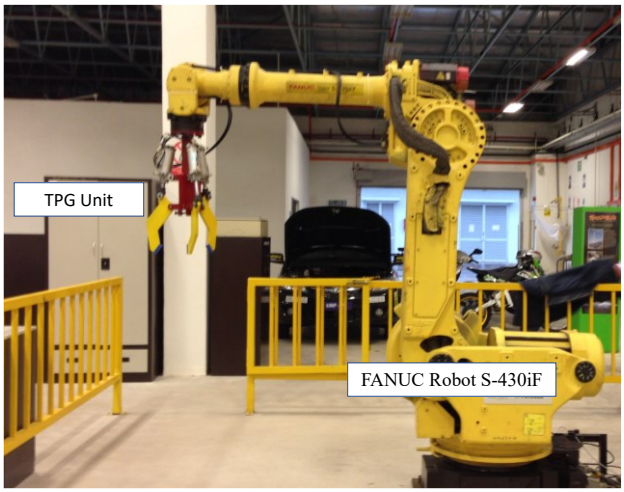

Fig. 1. Tri-finger Pneumatic Grasper (TPG) attached as a tool for FANUC S-430iF.

TPG is specified for industrial scale tasks including the picking and placing of large objects such as single carton, box, racks etc. This customized robot grasper was configured with three pneumatic pistons for each finger as purposed for the operation of two primary states: gripping state (GS) and release state (RS). One of the fingers was configured with Pneumatic Proportional Valve with Double-acting Cylinder (PPVDC) rod-piston to make it controllable and conveniently adaptable during its grasping operation. Detailed specification and configuration of TPG are listed in Table 1. As observed, the finger as operated by PPVDC was configured with multiple input and single-output (MISO) structure, where all the inputs come from 32-bit microcontroller within an embedded controller unit to the 5/3-way pneumatic proportional valve. In return, two feedback responses were generated from both the rotary encoder and pressure transducer as shown in Fig. 2.

TABLE I. LIST OF COMPONENTS AND EQUIPMENT IN TPG UNIT

Equipment	Value
Pneumatic cylinder	CKD Air Cylinder CAC4-A-50B-75-Y/Z
Pneumatic proportional valve	Festo MPYE-5-1/4-010-B
Pneumatic pressure regulator & filter	AirTAC SR200
Pneumatic pressure transducer	Festo SPTW-P10R-G14-A-M12
Air compressor	SWAN SVP202 Air Compressor
Rotary encoder	Rotary encoder - 500ppr

All sensors were connected to the customized conditioner circuit within the embedded controller board. The hardware-in-loop control approach was further deployed for this system using the MATLAB® SIMULINK software environment.

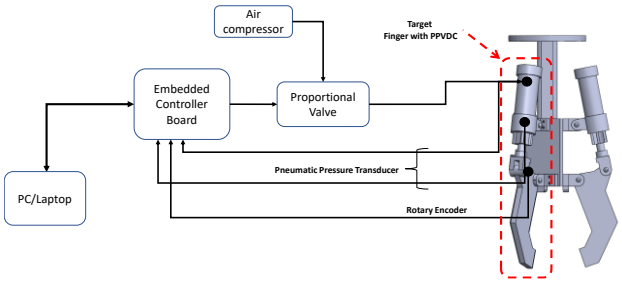

Fig. 2. TPG control system architecture for a finger with PPVDC.

III. INTERACTION MOTION CONTROL DESIGN

A. *Position-based Impedance Control Design with Pressure-based Force Estimation on Fingertip*

To achieve the objective of adaptive grasping, one of TPG's fingers has been designed with the proposed interaction motion control known as F-TIE. Based on the relationship in Eq. (1), detailed illustration as given in Fig. 3 further elaborates respective contact force from the environment (F_e) that reflects the finger's desired impedance behavior.

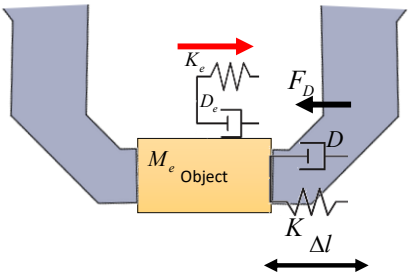

Fig. 3. TPG with impedance control and interacting with environment/ object surface

Practical emphasis was gravitated towards in-depth apprehension regarding interaction between equilibrium force as exerted via the fingertip and force as encountered from the environment or the object's surface.

$$D_f = M\Delta\ddot{l}(t) + D\Delta\dot{l}(t) + K\Delta l(t) \quad (1)$$

where

$$D_f = F_D - F_e \quad (2)$$

where F_D indicates the force from a finger which experienced actuation of a pneumatic piston. Both damper and stiffness of the desired impedance are represented by respective notations of D and K to constitute the system's elastic properties, whilst having M as the finger's mass. With reference to the illustration given in Fig. 4, translation displacement of the finger, l, in response to changes on its joint (θ) can be subsequently calculated from the structure's inverse kinematics through employment of Equation (3) as follows.

$$\theta = tan^{-1}\left(\frac{x}{y}\right) \quad (3)$$

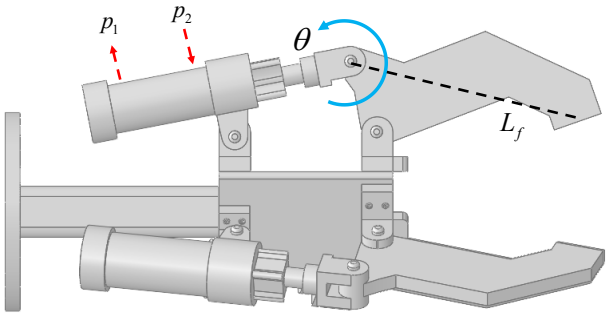

Fig. 4. TPG finger coordination.

where x and y represent axial motions of the finger, with $l = y$ following the illustration in Fig. 3. Dynamism of the fingertip as per illustrated in Fig. 5, D_f, was alternatively derived from the established relationship between torque as generated by the fingertip's joint, force within the cylinder and resultant forces on the tip (end-effector). Its expression was then outlined in Eq. (4).

$$D_f = [F_x \quad F_y]^T = J^{-T}(\tau_c + \tau_g) \quad (4)$$

where torque by cylinder (τ_{cyl}) was expressed as Eq. (5).

$$\tau_c = G_T F_P \quad (5)$$

force within the pneumatic cylinder (F_P) was determined from different pressures as outlined in Eq. (6).

$$F_p = P_1 A_1 - P_2 A_2 - P_{atm}(A_1 - A_2) \quad (6)$$

and the gravitational compensator [55] or torque gain (G_T) was determined from the geometry relation in Fig. 5 between the finger's sub-joint range (δ_1, δ_2), length of sub-links (l_1, l_2) and length of piston (H) as expressed in Eq. (7).

$$G_T = \frac{l_1 l_2 \, sin(\pi + \theta + \delta_1)}{H} \quad (7)$$

where

$$H = \sqrt{l_1^2 + l_2^2 - 2l_1 l_2 \, cos(\pi + \theta - \delta_1)}.$$

On the other hand, the gravitational torque (τ_g) was calculated through employment of Eq. (8) as follows.

$$\tau_g = JF_g = J[0 \quad m_L g] \quad (8)$$

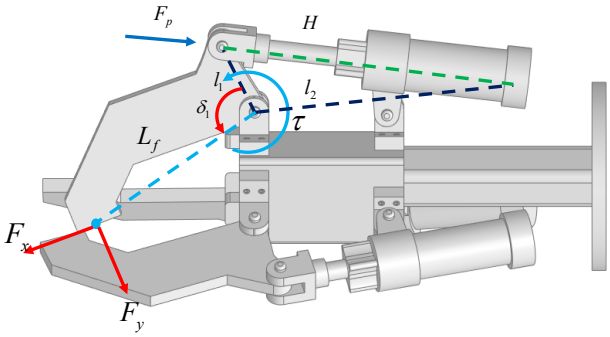

Fig. 5. The different forces and geometry that considered in proposed PFE for a TPG's tip.

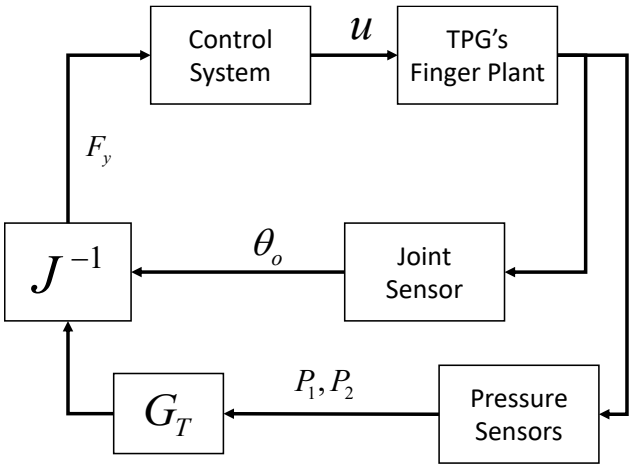

Fig. 6. Overall diagram on the proposed pressure-based force estimation on fingertip

Jacobian matrix (J) was used to relate actual rotation of velocity ($\dot{\theta}$) for the robot's finger to the tip axis velocity ($\dot{\Gamma}$). Stated relationship can be written as per Eq. (9).

$$\tau_g = JF_g = J[0 \quad m_L g] \quad (9)$$

where $J \in \mathbb{R}^{MxN}$ for this robot, with $M = 2$ and $N = 1$. The finger axes were further represented by $\Gamma = \{x, y\}$, with both notations of x and y being the kinematics of a single TPG finger that can be separately expressed through Eq. (10) and Eq. (11) as follows

$$x = SL_f \quad (10)$$

$$y = CL_f \quad (11)$$

where L_f denotes the length of TPG's finger, $S = \sin\theta$ and $C = \cos\theta$. Fixed values for each vertical sub-links and sub-joint range were determined in accordance with actual dimensions of the TPG as listed in Table 2. F_y was significantly considered as $D_f = kF_y$ under the principal structure and application of TPG, with k being a positive

constant compensator gain for the estimation output. Overall diagram for the proposed pressure-based force estimator as implemented to TPG's fingertip is shown as Fig. 6.

TABLE II. PARAMETER OF SINGLE FINGERTIP

Parameter	Value
l_1	0.076m
m_L	2kg
l_2	0.285
δ_1	118^0
L_f	0.225m

B. Variable Convergence Rate Prescribed Performance on Position-based Impedance Control

Conceptual idea of the variable rate convergence prescribed performance impedance control has emerged from the experienced imprecision in error tracking upon facing transformed trajectory across difference between desired input trajectory and impedance controller output. In other words, the desired input trajectory would constantly exhibit transformative uncertainty following contact between both the robot's fingertip and the environment with stiffness. Such situation can be expressed as Eq. (12).

$$e = \theta_r - \Delta\theta - \theta_o \tag{12}$$

where θ_r is a trajectory input from the robot system, $\Delta\theta$ is an inverse kinematic on y-axis motion of the impedance controller with reference to Eq. (11) and θ_o is a feedback finger joint rotational. According to the fundamental of PPC [35], a drawback was encountered at $t \to +\infty$ from PPF's inability to reach the boundary. Experienced difficulty centering speed of the convergence rate (h) further resulted a deviation to the desired h value regarding transient convergence rate of the decay function period. While such problem was previously overcome in [35-38], weakness remained on its fixed convergence rate. Therefore, the earlier FT-PPF was modified through adoption of the revised exponential properties as expressed in Eq. (12), with the predefined performance function $\rho(t)$ being a strictly decreasing smooth function, and $\lim_{t\to\infty}\rho(t) = \rho_\infty$.

$$\rho(t) = (\rho_0 - \rho_\infty)e^{-\nu} + p_\infty \tag{13}$$

where

$$\nu = \frac{2\alpha^2}{{t_0}^2} \tag{14}$$

and

$$\alpha = \lambda_1 t(tanh[\lambda_2(t - t_0) + 1]). \tag{15}$$

ρ_0 hereby indicates the baseline range of finite-time tracking error ($e(t)$) at the transient interval, whilst representing the maximum allowable range of $e(t)$ at the steady-state period, in which $\rho_0 > \rho_\infty > 0$. t_0 is the predetermined convergence finite-time, with $\lambda_1 \in \Re$ and $\lambda_2 \in \Re$ being the scaling factors for finite time and convergence rate, respectively.

According to the formulated finite-time prescribed performance in [37], control strategy for the position-based impedance control can be formulized and expressed as Eq. (16) through highlighting the relationship between decay function ($\rho(t)$) within Eq. (12).

$$e(t) = \rho(t)S(\varepsilon) \tag{16}$$

where

$$S(\varepsilon(t)) = \frac{\bar{\sigma}e^{\varepsilon(t)} - \underline{\sigma}e^{-\varepsilon(t)}}{e^{\varepsilon(t)} + e^{-\varepsilon(t)}} \tag{17}$$

and $\varepsilon(t)$ is the revised $e(t)$ for function $S(\varepsilon)$ which increases under strict monotonicity at the acquisition of $|e(t)| < \rho(t), \forall t \geq 0$. This function is also known by the bounded inverse transformation function of error which can be expressed as follows [36].

$$\varepsilon(t) = S^{-1}\left(\frac{e(t)}{\rho(t)}\right) = \frac{1}{2}ln\left(\frac{\psi(t)+1}{1-\psi(t)}\right) \tag{18}$$

where $S^{-1}(\bullet)$is the inverse function of $S(\varepsilon)$ with normalized error $\psi(t) = \frac{e(t)}{\rho(t)}$ at $|\varepsilon(0)| < 1$ under the specification of $-1 < \psi(t) < 1$ when $\varepsilon(t) \neq \infty$. Fig. 7 further illustrates a detailed blueprint of the variable convergence rate prescribe performance impedance control (VPPIC).

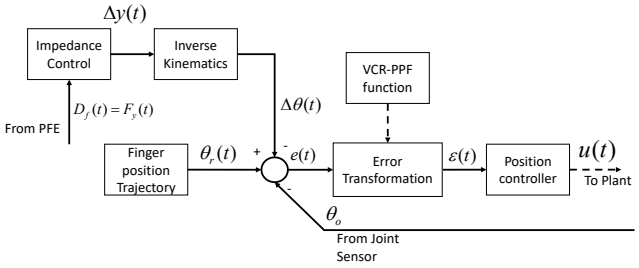

Fig. 7. Detail diagram for the proposed VPPIC.

The predefined bound for PPF [35] would be guaranteed under the condition where $\varepsilon(t)$ is constantly bounded. Such arrangement then steered the control objective towards fabrication of both impedance and position controls which ensure a bounded $\varepsilon(t)$. While the response of $e(t)$ is not affected by the boundary value of $\varepsilon(t)$, it is determined by Eq. (16) with a pre-defined $\rho(t)$. Overall control design for VPPIC with the proposed PFE on a finger of TPG is then detailed in Fig. 8.

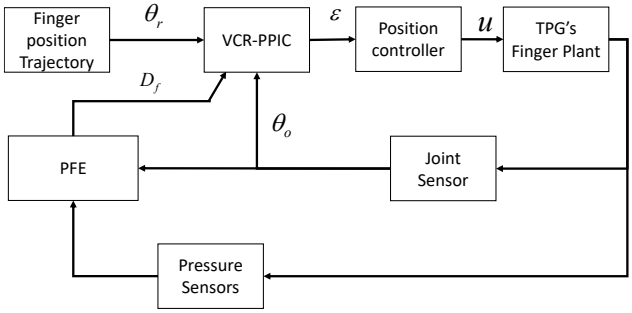

Fig. 8. Overall control diagram for a single TPG's fingertip with proposed VPPIC and PFE.

IV. EXPERIMENT AND RESULTS

As shown in Fig. 9, the proposed VPPIC with PFE was verified and validated on a finger of the TPG robot through employment of a ping-pong ball as the grasped target. Undertaken experiment then commenced with calibration of the proposed PFE as a touching force feedback.

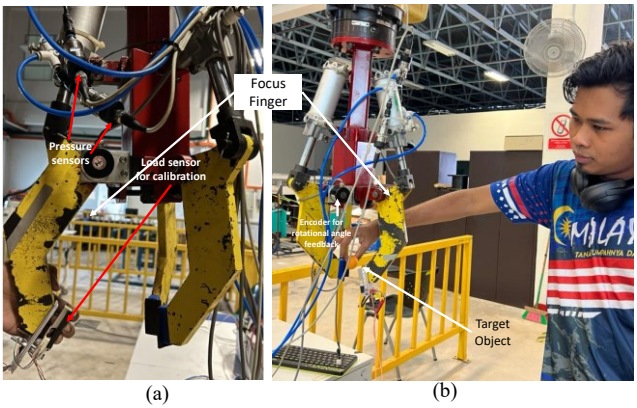

Fig. 9. Experiment setup for a TPG's fingertip; (a) PFE calibration setup, (b) VPPIC test setup

With reference to Fig. 10, the calibration was undertaken through comparison of output D_f to measured results from the loadcell as attached on TPG's fingertip. Acquired final values succeeding fine-tuning of PFE's output gain, k, are further listed in Table 3. As depicted in Fig. 10(a), basic open-and-close (free GS and RS running) operations of the finger were executed. Tested motions were simultaneously restricted by application of the barehand as a blockage at arbitrary intervals to test its sensory effect. Recorded outcomes from both the estimator and sensor are collectively tabulated through the red-dotted line in Fig. 11 as specified by notation FS.

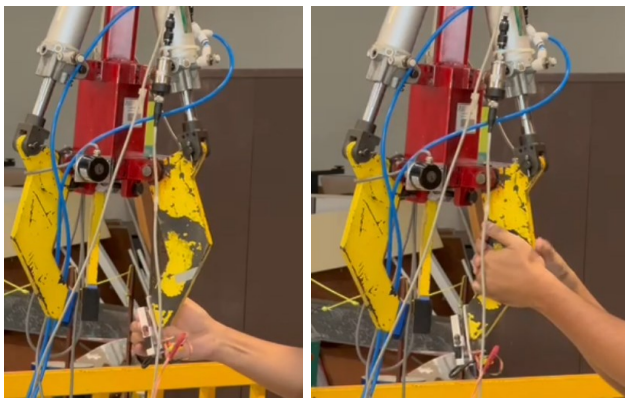

Fig. 10. Snapshot of validation for proposed force estimator (a) pushing only fingertip, (b) pulling finger

Obtained results as conjointly exhibited in Fig. 11 has suggested overpowering accuracy of PFE towards estimation of the true value against its FS counterpart at a smaller predictive error of 2%. Acquired force estimation output is hereby depicted in Fig. 12 with accordance to the interaction between both joint angular of the finger and pressure within the pneumatic piston with compensator G_T. Recognized as a major element across investigated estimation methods with artifical intelligence in [56-58], the processing interval has been optimized in response to the exclusion of iteration process from its algorithmic settings. Sole mechanistic implementation of the structure's geometry and Jacobian for the currently examined method has also guaranteed reduced modelling complexity against the comparable works of [11, 12, 59, 60] where actual sensor reading was selectively applied for results verification. With reference to Fig. 10(b), obtained results on the finger's pull-and-release operation under the implementation of PFE have been tabulated in Fig. 13. Notable force feedback response is subsequently observed beyond sensory capacity on the system's fingertip upon surpassing of 230 secs the stimulated interval. Demonstrated outcomes on both fingertip and finger collision sensing, thus, confirmed the effectiveness of PFE towards finger-wide sensing.

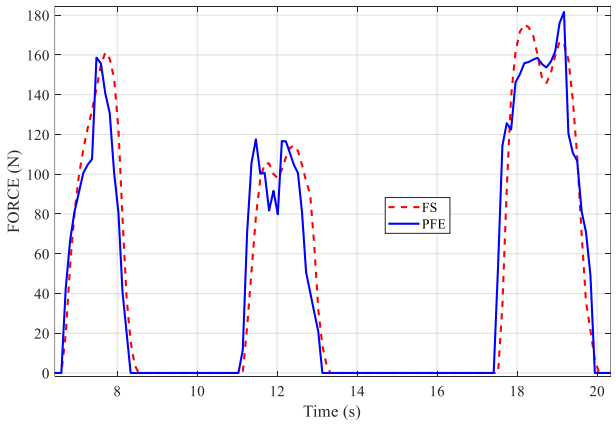

Fig. 11. Sample of F_y between ouput from PFE and loadcell reading.

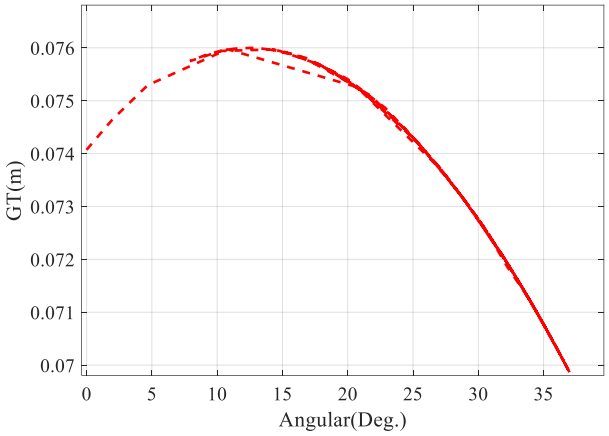

Fig. 12. Sample of F_y between ouput from PFE and loadcell reading.

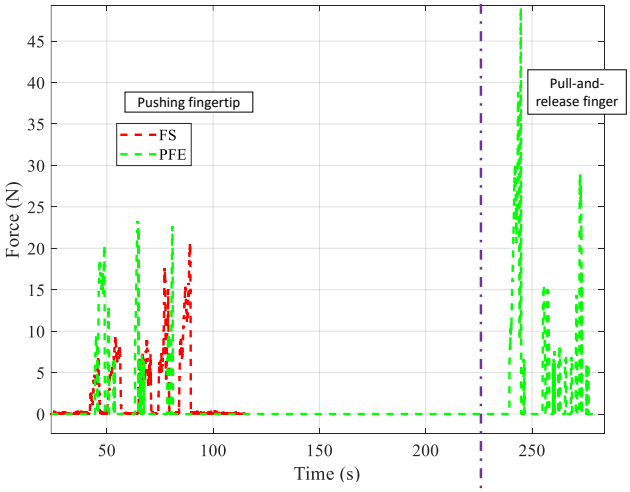

Fig. 13. Sample of force responses for PFE vs. FS.

With reference to Fig. 14, subsequent experimentation was executed on the grasp-and-release operation with a ping-pong ball as the grasped target to validate the proposed VPPIC. Comparison was made between the proposed method and the standard position-based impedance through uniform application of the fine-tuned FOPID [36] as their position control. As such, values for the optimized parameters for FOPID, VPPIC and the standard impedance control have been collectively listed in Table 3, with demonstrated improvement and reliability of the proposed method being separately presented through the results in Fig. 15. Correspond to the sustained tracking error on in bound motion without observable oscillation between both 10 and 15 secs of the sample results, obtained findings from the implementation of VPPIC especially exhibited an increasingly controllable tracking error against IC with respect to the ball's position following executed interaction.

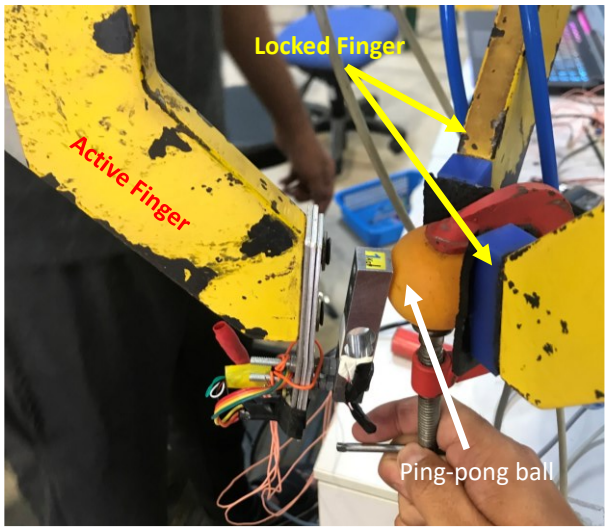

Fig. 14. VPPIC experimental setup.

TABLE III. FINE-TUNED CONTROLLER'S PARAMETER VALUES

Controller	Parameter	Value
FOPID	K_P	1.115
	K_i	0.352
	K_d	0.0390
	λ	0.2
	μ	0.15
VPPIC	M	2
	K	5
	D	2
	ρ_0	55
	ρ_∞	3
	t_0	0.5
	$\bar{\sigma}$	1
	$\underline{\sigma}$	1
	λ_1	1
	λ_2	1
PFE	k	100

Similarly observed in Fig. 16, a marginally greater different pressure of 2MPa against IC is further overshadowed by the minimal jerking in pressure from VPPIC. Such results have continued to exert consequential repercussion on the force feedback response in Fig. 17 following a considerably smoother D_f from VPPIC apropos a significantly longer finger-object interaction of approximately 3 to 5 seconds over its IC counterpart at an average force of 350N. A prolonged contact, therefore, prevailed VPPIC as the more reliable alternative for gentle and compression-free object gripping at specified stiffness.

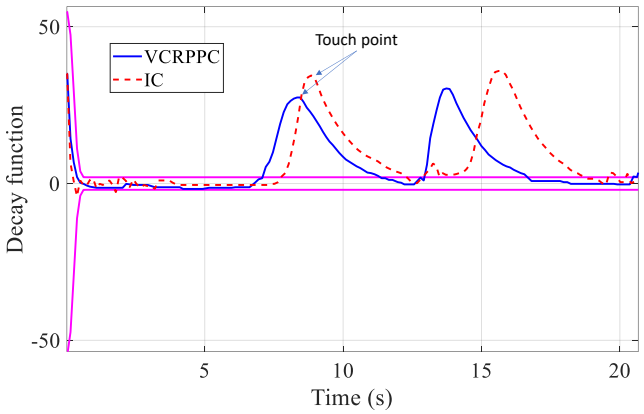

Fig. 15. Sample of tracking error performance with prescribed performance bound of the rod-piston between VPPIC and IC.

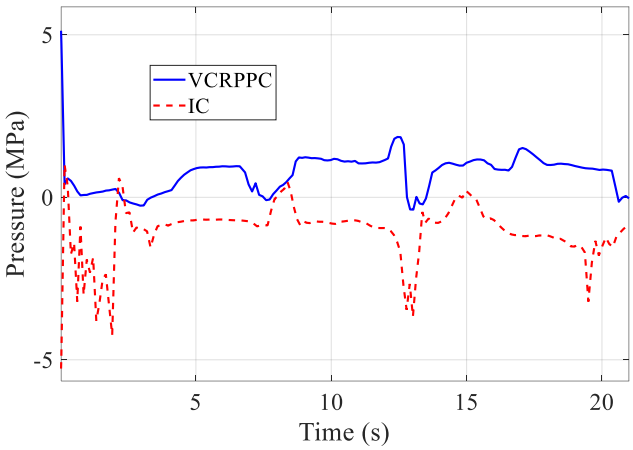

Fig. 16. Sample of pressure difference performance between VPPIC and IC.

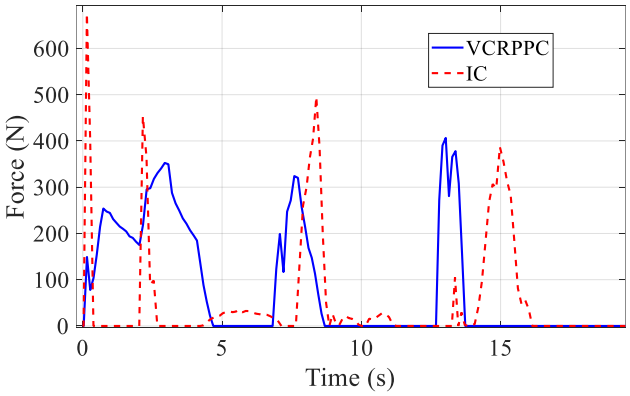

Fig. 17. Sample of F_y between output from PFE between the VPPIC and IC.

V. CONCLUSION

Current proposition specified the implementation of VPPIC for an interaction control on a finger of TPG robot

with PFE. System's competency towards environmental interaction at the absence of force/load sensor on the fingertip was showcased through the experimented impedance control with force estimator. Recommended estimation further expanded sensory capacity beyond the fingertip to seclude its entire finger. Additionally, VPPIC has demonstrated stable interactive motion against fragile object as represented by a ping-pong ball towards various impedance control behaviors with variable convergence rates for prescribed performance on overall tracking error from both position and impedance model. Nevertheless, sustainability of a stable interaction control on fragile object operation by heavy-duty industrial robots is not guaranteed on the account of static controlling boundaries such as impedance control. Such revelation then steered future research within this context towards exploratory improvement of the prescribed performance control.

ACKNOWLEDGMENT

Deepest gratitude is directed to the Ministry of Higher Education for the financial support as provided under Fundamental Research Grant Scheme (FRGS) No. FRGS/1/2019/TK04/UMP/02/1 (University reference RDU1901106), as well as Universiti Malaysia Pahang for the laboratorial facilities and financial assistance as offered under the Postgraduate Research Grant (PGRS2003158).

REFERENCES

[1] X. Zhao, B. Tao, L. Qian, Y. Yang, and H. Ding, "Asymmetrical nonlinear impedance control for dual robotic machining of thin-walled workpieces," *Robotics and Computer-Integrated Manufacturing,* vol. 63, p. 101889, 2020.

[2] T. Wang, T. Zhang, A. Song, and Y. Zhang, "An input shaping based active vibration control and adaptive RBF impedance control for suppressing the myospasm in upper-limb rehabilitation," *Applied Soft Computing,* p. 106380, 2020.

[3] K. Xu, S. Wang, B. Yue, J. Wang, H. Peng, D. Liu*, et al.*, "Adaptive impedance control with variable target stiffness for wheel-legged robot on complex unknown terrain," *Mechatronics,* vol. 69, p. 102388, 2020.

[4] N. M. Adam, A. Irawan, and F. K. Faudzi, "Impedance control on rack steering vehicle for inertia shaping on cornering track," *International Journal of Dynamics and Control,* vol. 7, pp. 1434-1442, 2019.

[5] W. M. N. W. Lezaini, A. Irawan, and A. R. Razali, "Impedance Control Approach on Leg Motion Speed Variation on Soft Surface Interaction," *International Journal of Engineering and Technology (UAE),* vol. 7, pp. 16-21, 2018.

[6] R. Wu, H. Zhang, T. Peng, L. Fu, and J. Zhao, "Variable impedance interaction and demonstration interface design based on measurement of arm muscle co-activation for demonstration learning," *Biomedical Signal Processing and Control,* vol. 51, pp. 8-18, 2019.

[7] N. Hogan, "Impedance Control: An Approach to Manipulation," in *American Control Conference, 1984*, 1984, pp. 304-313.

[8] A. Toedtheide, T. Lilge, and S. Haddadin, "Antagonistic Impedance Control for Pneumatically Actuated Robot Joints," *IEEE Robotics and Automation Letters,* vol. 1, pp. 161-168, 2016.

[9] M. I. P. Azahar, A. Irawan, R. M. Taufika, and M. H. Suid, "Position Control of Pneumatic Actuator Using Cascade Fuzzy Self-adaptive PID," Singapore, 2020, pp. 3-14.

[10] M. I. P. Azahar, A. Irawan, and R. M. T. R. Ismail, "Self-tuning hybrid fuzzy sliding surface control for pneumatic servo system positioning," *Control Engineering Practice,* vol. 113, p. 104838, 2021.

[11] A. Wahrburg, E. Morara, G. Cesari, B. Matthias, and H. Ding, "Cartesian contact force estimation for robotic manipulators using Kalman filters and the generalized momentum," in *2015 IEEE International Conference on Automation Science and Engineering (CASE)*, 2015, pp. 1230-1235.

[12] Y. Xin, H. Chai, Y. Li, X. Rong, B. Li, and Y. Li, "Speed and Acceleration Control for a Two Wheel-Leg Robot Based on Distributed Dynamic Model and Whole-Body Control," *IEEE Access,* vol. 7, pp. 180630-180639, 2019.

[13] J. Jo, G. Park, and Y. Oh, "Robust walking stabilization strategy of humanoid robots on uneven terrain via QP-based impedance/admittance control," *Robotics and Autonomous Systems,* vol. 154, p. 104148, 2022.

[14] H. Ochoa and R. Cortesão, "Impedance control architecture for robotic-assisted micro-drilling tasks," *Journal of Manufacturing Processes,* vol. 67, pp. 356-363, 2021.

[15] A. Marban, V. Srinivasan, W. Samek, J. Fernández, and A. Casals, "A recurrent convolutional neural network approach for sensorless force estimation in robotic surgery," *Biomedical Signal Processing and Control,* vol. 50, pp. 134-150, 2019.

[16] R. Rashad, D. Bicego, R. Jiao, S. Sanchez-Escalonilla, and S. Stramigioli, "Towards Vision-Based Impedance Control for the Contact Inspection of Unknown Generically-Shaped Surfaces with a Fully-Actuated UAV," in *2020 IEEE/RSJ International Conference on Intelligent Robots and Systems (IROS)*, 2020, pp. 1605-1612.

[17] V. Lippiello, G. A. Fontanelli, and F. Ruggiero, "Image-Based Visual-Impedance Control of a Dual-Arm Aerial Manipulator," *IEEE Robotics and Automation Letters,* vol. 3, pp. 1856-1863, 2018.

[18] C. Vidrios-Serrano, M. Mendoza, I. Bonilla, and B. Maldonado-Fregoso, "A Generalized Vision-based Stiffness Controller for Robot Manipulators with Bounded Inputs," *International Journal of Control, Automation and Systems,* vol. 19, pp. 548-561, 2021.

[19] S. Liu, L. Wang, and X. V. Wang, "Sensorless force estimation for industrial robots using disturbance observer and neural learning of friction approximation," *Robotics and Computer-Integrated Manufacturing,* vol. 71, p. 102168, 2021.

[20] W. Ji, J. Zhang, B. Xu, C. Tang, and D. Zhao, "Grasping mode analysis and adaptive impedance control for apple harvesting robotic grippers," *Computers and Electronics in Agriculture,* vol. 186, p. 106210, 2021.

[21] K. Nonami, R. K. Barai, A. Irawan, and M. R. Daud, "Impedance Control and Its Adaptive for Hexapod Robot," in *Hydraulically Actuated Hexapod Robots*, 2014, pp. 169-197.

[22] A. Irawan, K.Nonami, M.R.Daud, "Optimal Impedance Control with TSK-type FLC for Hard Shaking Reduction on Hydraulically Driven Hexapod Robot," in *Proceeding of The International Conference on Intelligent Unmanned Systems 2011 (ICIUS 2011)*, 2011.

[23] P. Balatti, D. Kanoulas, G. F. Rigano, L. Muratore, N. G. Tsagarakis, and A. Ajoudani, "A Self-Tuning Impedance Controller for Autonomous Robotic Manipulation," in *2018 IEEE/RSJ International Conference on Intelligent Robots and Systems (IROS)*, 2018, pp. 5885-5891.

[24] M. H. Hamedani, M. Zekri, F. Sheikholeslam, M. Selvaggio, F. Ficuciello, and B. Siciliano, "Recurrent fuzzy wavelet neural network variable impedance control of robotic manipulators with fuzzy gain dynamic surface in an unknown varied environment," *Fuzzy Sets and Systems,* 2020.

[25] X. Zhang, T. Sun, and D. Deng, "Neural approximation-based adaptive variable impedance control of robots," *Transactions of the Institute of Measurement and Control,* vol. 42, pp. 2589-2598, 2020.

[26] A. Liu, T. Chen, H. Zhu, M. Fu, and J. Xu, "Fuzzy variable impedance-based adaptive neural network control in physical human–robot interaction," *Proceedings of the Institution of Mechanical Engineers, Part I: Journal of Systems and Control Engineering*, 2022.

[27] A. Irawan, M. M. Alam, and Y. Y. Tan, "PD-FLC with admittance control for hexapod robot's leg positioning on seabed," in *2015 10th Asian Control Conference (ASCC)*, 2015, pp. 1-5.

[28] M. M. Alam, A. Irawan, and T. Y. Yin, "Buoyancy effect control in multi legged robot locomotion on seabed using integrated impedance-fuzzy logic approach," *Indian Journal of Geo-marine Science* vol. 44, pp. 1937-1945, 2015.

[29] M. U. Masood and M. Haghshenas-Jaryani, "A Study on the Feasibility of Robotic Harvesting for Chile Pepper," *Robotics,* vol. 10, p. 94, 2021.

[30] A. Izadbakhsh, S. Khorashadizadeh, and S. Ghandali, "Robust adaptive impedance control of robot manipulators using Szász–Mirakyan operator as universal approximator," *ISA Transactions,* 2020.

[31] W. Ji, C. Tang, B. Xu, and G. He, "Contact force modeling and variable damping impedance control of apple harvesting robot," *Computers and Electronics in Agriculture,* vol. 198, p. 107026, 2022.

[32] M. Beschi, E. Villagrossi, L. M. Tosatti, and D. Surdilovic, "Sensorless model-based object-detection applied on an underactuated adaptive

hand enabling an impedance behavior," *Robotics and Computer-Integrated Manufacturing,* vol. 46, pp. 38-47, 2017.

[33] J. Slightam, E. Barth, and M. Nagurka, "Sliding Mode Impedance and Stiffness Control of a Pneumatic Cylinder," *ASME 2019 Dynamic Systems and Control Conference*, 2019, pp. 1-8.

[34] M. Turkseven and J. Ueda, "Observer based impedance control of a pneumatic system with long transmission lines," in *2016 IEEE International Conference on Robotics and Automation (ICRA)*, 2016, pp. 1160-1165.

[35] M. I. P. Azahar, A. Irawan, and M. S. Ramli, "Finite-Time Prescribed Performance Control for Dynamic Positioning of Pneumatic Servo System," in *2020 IEEE 8th Conference on Systems, Process and Control (ICSPC)*, 2020, pp. 1-6.

[36] M. I. P. Azahar, A. Irawan, and M. S. Ramli, "Transient Control Improvement on Pneumatic Servoing in Robot System using Fractional-Order PID with Finite-time Prescribed Performance Control," in *2022 IEEE 12th Symposium on Computer Applications & Industrial Electronics (ISCAIE)*, 2022, pp. 206-210.

[37] M. I. P. Azahar and A. Irawan, "Enhancing Precision on Pneumatic Actuator Positioning using Cascaded Finite-time Prescribed Performance Control," in *2021 11th IEEE International Conference on Control System, Computing and Engineering (ICCSCE)*, 2021, pp. 131-136.

[38] A. Irawan, M. I. P. Azahar, and Z. H. Ismail, "Interaction Motion on Pneumatic Cylinder using Prescribed Performance Force Tracking Impedance Control," in *2020 8th International Conference on Control, Mechatronics and Automation (ICCMA)*, 2020, pp. 121-126.

[39] K. Wang, T. Meng, W. Wang, R. Song, and Z. Jin, "Finite-time extended state observer based prescribed performance fault tolerance control for spacecraft proximity operations," *Advances in Space Research,* vol. 70, pp. 1270-1284, 2022.

[40] X. Bu, B. Jiang, and Y. a. Feng, "Hypersonic tracking control under actuator saturations via readjusting prescribed performance functions," *ISA Transactions,* 2022.

[41] H. Liu, Q. Cheng, J. Xiao, and L. Hao, "Data-driven optimal tracking control for SMA actuated systems with prescribed performance via reinforcement learning," *Mechanical Systems and Signal Processing,* vol. 177, p. 109191, 2022.

[42] D. Liu and G. H. Yang, "Prescribed Performance Model-Free Adaptive Integral Sliding Mode Control for Discrete-Time Nonlinear Systems," *IEEE Transactions on Neural Networks and Learning Systems,* vol. 30, pp. 2222-2230, 2019.

[43] G. Luo, H. Li, B. Ma, and Y. Wang, "Design and experimental research of observer-based adaptive type-2 fuzzy steering control for automated vehicles with prescribed performance," *Mechatronics,* vol. 81, p. 102700, 2022.

[44] X. Cao, J. Wang, and W. Xiang, "Composite Adaptive Fuzzy Prescribed Performance Control of Nonlinear Systems," *Mathematical Problems in Engineering,* vol. 2020, p. 2948130, 2020.

[45] X. Bu, "Prescribed performance control approaches, applications and challenges: A comprehensive survey," *Asian Journal of Control,* 2021.

[46] N.-N. Zhao, A.-M. Zhang, X.-Y. Ouyang, L.-B. Wu, and H.-B. Xu, "A novel prescribed performance controller for strict-feedback nonlinear systems with input constraints," *ISA Transactions,* 2022.

[47] Y. Wang, G. Luo, and D. Wang, "Observer-based fixed-time adaptive fuzzy control for SbW systems with prescribed performance," *Engineering Applications of Artificial Intelligence,* vol. 114, p. 105026, 2022.

[48] Z. Namadchian and M. Rouhani, "Adaptive prescribed performance neural network control for switched stochastic pure-feedback systems with unknown hysteresis," *Neurocomputing,* vol. 429, pp. 151-165, 2021.

[49] L. Chang, Y. Jing, and Y. Liu, "Design of adaptive H∞ controller for power system based on prescribed performance," *ISA Transactions,* vol. 100, pp. 244-250, 2020.

[50] B. Sánchez-García, F. Reyes-Cortés, B. Al-Hadithi, and O. Félix-Beltrán, "Global Saturated Regulator with Variable Gains for Robot Manipulators," *Journal of Robotics and Control (JRC),* vol. 2, no. 6, 2021.

[51] X. Bu, G. He, and D. Wei, "A new prescribed performance control approach for uncertain nonlinear dynamic systems via back-stepping," *Journal of the Franklin Institute,* vol. 355, pp. 8510-8536, 2018.

[52] S. Gao, X. Liu, Y. Jing, and G. M. Dimirovski, "A novel finite-time prescribed performance control scheme for spacecraft attitude tracking," *Aerospace Science and Technology,* vol. 118, p. 107044, 2021.

[53] J. Lin, H. Liu, and X. Tian, "Neural network-based prescribed performance adaptive finite-time formation control of multiple underactuated surface vessels with collision avoidance," *Journal of the Franklin Institute,* vol. 359, pp. 5174-5205, 2022.

[54] S. Luo, X. Wu, C. Wei, Y. Zhang, and Z. Yang, "Adaptive finite-time prescribed performance attitude tracking control for reusable launch vehicle during reentry phase: An event-triggered case," *Advances in Space Research,* vol. 69, pp. 3814-3827, 2022.

[55] K. Nonami, R. K. Barai, A. Irawan, and M. R. Daud, "Kinematics, Navigation, and Path Planning of Hexapod Robot," *Hydraulically Actuated Hexapod Robots*, pp. 85-104, 2014.

[56] A.-N. Sharkawy, P. N. Koustoumpardis, and N. A. Aspragathos, "Human–robot collisions detection for safe human–robot interaction using one multi-input–output neural network," *Soft Computing,* vol. 24, pp. 6687-6719, 2020.

[57] J. Luo, C. Liu, and C. Yang, "Estimation of EMG-Based Force Using a Neural-Network-Based Approach," *IEEE Access,* vol. 7, pp. 64856-64865, 2019.

[58] F. Wang, Y. Jiang, Y. Song, S. Lv, M. Li, and R. Ye, "Visual Interaction Force Estimation Based on Time-Sensitive Dual-Resolution Learning Network," *Journal of Sensors,* vol. 2022, p. 4302179, 2022.

[59] C. P. Vo and K. K. Ahn, "An Adaptive Finite-Time Force-Sensorless Tracking Control Scheme for Pneumatic Muscle Actuators by an Optimal Force Estimation," *IEEE Robotics and Automation Letters,* vol. 7, pp. 1542-1549, 2022.

[60] P. Cheng, J. Jia, Y. Ye, and C. Wu, "Modeling of a Soft-Rigid Gripper Actuated by a Linear-Extension Soft Pneumatic Actuator," *Sensors,* vol. 21, p. 493, 2021.